

Article

Enhanced SO₂ Resistance of Cs-Modified Fe-HZSM-5 for NO Decomposition

Fan Wang¹, Pengfei Liu¹, Jiaxue Guo¹, Kexin Xu¹, Yanrui Zhang¹, Yanhui Yi² , Yimin Zhu¹ and Li Wang^{1,*} ¹ College of Environmental Sciences and Engineering, Dalian Maritime University, Dalian 116026, China² State Key Laboratory of Fine Chemicals, School of Chemical Engineering, Dalian University of Technology, Dalian 116024, China

* Correspondence: liwang@dmlu.edu.cn; Tel.: +86-411-84724357

Abstract: Direct decomposition of NO into N₂ and O₂ is an ideal technology for NO_x removal. Catalyst deactivation by sulfur poisoning is the major obstacle for practical application. This paper focuses on strengthening the SO₂ resistance of metal-exchanged HZSM-5 catalysts, by investigating the metals, promoters, preparation methods, metal-to-promoter molar ratios, Si/Al ratios and metal loadings. The results show that in the presence of SO₂ (500 ppm), Fe is the best compared with Co, Ni and Cu. Cs, Ba and K modification enhanced the low-temperature activity of the Fe-HZSM-5 catalyst for NO decomposition, which can be further improved by increasing the exchanged-solution concentration and Fe/Cs molar ratio or decreasing the Si/Al molar ratio. Interestingly, Cs-doped Fe-HZSM-5 exhibited a high NO conversion and low NO₂ selectivity but a high SO₂ conversion within 10 h of continuous operation. This indicates that Cs-Fe-HZSM-5 has a relatively high SO₂ resistance. Combining the characterization results, including N₂ physisorption, XRD, ICP, XRF, UV-Vis, XPS, NO/SO₂-TPD, H₂-TPR and HAADF-STEM, SO₄²⁻ was found to be the major sulfur species deposited on the catalyst's surface. Cs doping inhibited the SO₂ adsorption on Fe-HZSM-5, enhanced the Fe dispersion and increased the isolated Fe and Fe-O-Fe species. These findings could be the primary reasons for the high activity and SO₂ resistance of Cs-Fe-HZSM-5.

Keywords: NO decomposition; Fe-exchanged HZSM-5; Cs modification; SO₂ resistance

Citation: Wang, F.; Liu, P.; Guo, J.; Xu, K.; Zhang, Y.; Yi, Y.; Zhu, Y.; Wang, L. Enhanced SO₂ Resistance of Cs-Modified Fe-HZSM-5 for NO Decomposition. *Catalysts* **2022**, *12*, 1579. <https://doi.org/10.3390/catal12121579>

Academic Editor: Zhaoyang Fan

Received: 11 November 2022

Accepted: 2 December 2022

Published: 5 December 2022

Publisher's Note: MDPI stays neutral with regard to jurisdictional claims in published maps and institutional affiliations.



Copyright: © 2022 by the authors. Licensee MDPI, Basel, Switzerland. This article is an open access article distributed under the terms and conditions of the Creative Commons Attribution (CC BY) license (<https://creativecommons.org/licenses/by/4.0/>).

1. Introduction

The maritime transportation industry is the major driving force of the global economy. Currently, more than 90% of the world's trade is conducted by international shipping [1], which emits harmful gases, such as SO_x (sulfur oxides), NO_x (nitrogen oxides), CO₂ (carbon dioxide) and PM (particulate matter), due to the use of cheap low-quality fuels. Thus, ship emission pollution seriously affects the natural environment and human health [1–3].

The International Maritime Organization (IMO) has been inspecting ship emission pollution since 1988, and it has already established specific regulations to limit ship emission pollution. For example, the “International Convention for the Prevention of Pollution from Ships” Annex VI (MAPPOL 73/78/79) was passed in 1997, which has been constantly revised and imposed stricter restrictions on SO_x and NO_x emission in 2008 and 2019, respectively [1]. Currently, the limitation of SO_x emission from ship exhaust entered into force on a global maritime transportation scale on 1 January 2020, whereas NO_x emission from ship exhaust was planned to be reduced by 80% in the Baltic Sea and the North Sea, as the NECA area, after 1 January 2021 [4]. Until now, the technologies for maritime NO_x emission reduction have not been well-established due to the complexity of actual operation conditions.

The most desirable method for maritime NO_x removal is to directly decompose NO into harmless N₂ and O₂, due to cost-effectiveness, process simplicity and eco-friendliness, because it does not require any reductants such as NH₃, urea or hydrocarbons. From the

thermodynamic viewpoint, NO decomposition is favored, i.e., $\Delta G = -86$ kJ/mol [5], but is limited by dynamics due to the high activation energy of 364 kJ/mol [6]. Therefore, it is generally accepted that an efficient catalyst is the key to lower the energy barrier. Unfortunately, all reported catalysts, i.e., noble metals, metal oxides, perovskite-type oxides and zeolites, suffer from “oxygen inhibition”, caused by the strong chemisorption of superficial oxygen, which finally results in catalyst deactivation. This deactivation is more severe for noble metals, metal oxides and perovskite-type oxides. To accelerate O₂ desorption from the active sites, a high reaction temperature (>600 °C) is required for these catalysts [7–10].

Cu-based zeolite catalysts exhibit a relatively high activity of NO decomposition at low temperature due to a weaker “oxygen inhibition”, especially for the Cu-ZSM-5 catalyst. In 1986, Iwamoto et al. first reported a 90% NO decomposition at 450 °C using a Cu-ZSM-5 catalyst, which shows a higher resistance to “oxygen inhibition” in comparison with noble metals and metal oxides [11]. Since then, a lot of attention has been paid to Cu-ZSM-5 catalysts, and most studies focus on understanding the reaction mechanism, adjusting the hydrothermal stability and regulating the copper species through zeolite topology, preparation methods, Si/Al molar ratios and metal modifications in the absence of SO₂ [7–10].

Existing studies on NO catalytic decomposition are mostly performed under relatively mild conditions, but the ship exhaust gas is unstable, complex and rich in SO₂, ca. 500 ppm. More importantly, to avoid reheating of the ship exhaust gas, the devices for NO_x abatement have to be located upstream of the wet-scrubbing desulfurizer. That is, ship exhaust gas with SO₂ first passes through a catalyst bed that is used for DeNO_x, which makes the catalyst strongly deactivated by SO₂. Therefore, the SO₂ resistance of the catalyst has always been the biggest obstacle for practical application, and developing a SO₂-resistant catalyst for NO decomposition is indispensable for maritime NO_x removal.

However, the resistance to SO₂ of Cu-ZSM-5 has seldom been carried out. Iwamoto et al. found that Cu-ZSM-5 displays a very poor resistance to SO₂ poisoning, and the catalyst deactivated completely at 673–923 K [12]. In recent years, Fe-based catalysts were extensively investigated in the NH₃-SCR reaction, exhibiting a better sulfur-tolerant property than Cu-based catalysts [13–20]. However, only a few studies reported Fe-based catalysts for NO decomposition, and, furthermore, the sulfur resistance of Fe-based catalysts was also missed in these studies [21–24].

This study focuses on developing Fe-based HZSM-5 catalysts with a high SO₂ resistance, by adjusting the metals, promoters, preparation methods, metal/promoter molar ratios, Si/Al molar ratios and metal loadings. The activity of NO decomposition and SO₂ resistance of the prepared samples are evaluated under the conditions of simulated ship exhausts with 1000 ppm NO, 500 ppm SO₂ and 10 vol.% O₂ with N₂ as the balance gas. The catalysts are characterized by N₂ physisorption, XRD, ICP, XRF, UV-Vis, XPS, NO/SO₂-TPD, H₂-TPR and HAADF-STEM. Finally, the role of Cs as the best promoter in improving activity and the SO₂ resistance of Fe-HZSM-5 are discussed.

2. Results

This paper focuses on the SO₂ resistance of the prepared zeolite catalysts. Thus, the catalysts were exposed to a high concentration of SO₂, ca. 500 ppm, for all the tests. A series of strategies were adopted to improve the SO₂ resistance of Fe-HZSM-5 catalyst for achieving a superior performance for NO decomposition. Here, SO₂ conversion was used to evaluate the SO₂ resistance of catalysts. That is, a high conversion of SO₂ (i.e., a low SO₂ concentration in the outlet gas) presents a high sulfur deposition on the catalyst's surface.

2.1. NO Decomposition Activity of Metal-Exchanged HZSM-5 Catalysts

Figure 1 shows the influence of the exchanged metals on NO conversion, SO₂ conversion, and the by-product NO₂ formed during NO decomposition. However, no N₂O was observed over metal-exchanged HZSM-5 catalysts at 300–550 °C in this study. As presented

in Figure 1a, pure HZSM-5 had a very low NO conversion, whereas metal-exchanged HZSM-5 catalysts significantly enhanced the conversion of NO. The Fe-exchanged sample exhibited the highest NO conversion among the Fe-, Co-, Ni- and Cu-exchanged samples. Meanwhile, by-product NO₂ was produced, and its selectivity changed with metal type, which was observed to be a negative value in the case of pure HZSM-5, as shown in Figure 1b. The negative value mainly originated from the co-contribution of NO₂ formation and consumption, according to the calculation equation of NO₂ selectivity that is shown in Section 4.3. That is, no extra NO₂ was produced in the absence of a metal active site; meanwhile, some NO₂ molecules that existed in the feed gas were adsorbed by the HZSM-5 zeolite, which is rich in micropores. Additionally, metal-exchanged HZSM-5 led to sulfur deposition on the surface of the catalyst, as confirmed by the SO₂ conversion shown in Figure 1c, which changed with the metal type as well. In addition, reaction temperature had a significant influence on the catalytic activity of the metal-exchanged catalysts. NO conversion firstly increased then decreased, and a similar changing trend was observed for SO₂ conversion, though the temperatures at the turning points of NO conversion and SO₂ removal were different. For the best Fe-HZSM-5 catalyst, the optimal temperature is 350 °C, which corresponds to a high NO conversion but a low SO₂ deposition.

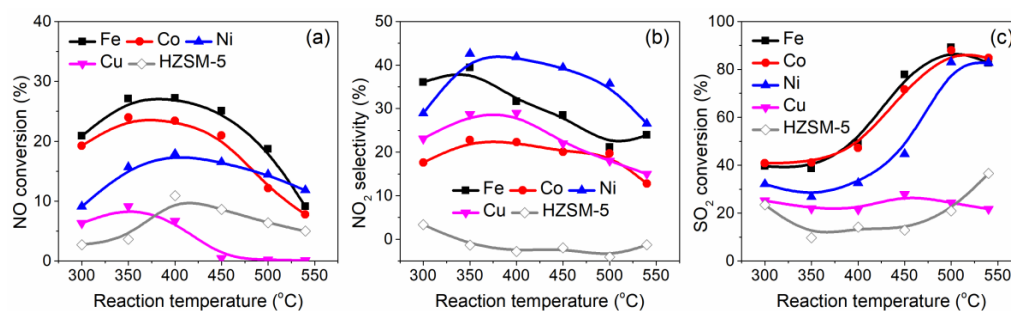


Figure 1. NO decomposition activity of metal-exchanged HZSM-5: (a) NO conversion; (b) NO₂ selectivity; (c) SO₂ conversion. NO = 1000 ppm, SO₂ = 500 ppm, O₂ = 10 vol.% with N₂ as balance gas, GHSV = 15,000 h⁻¹.

2.2. NO Decomposition Activity of Promoter-Doped Fe-HZSM-5

To strengthen the activity of the Fe-HZSM-5 catalyst for NO decomposition, various promoters were employed to modify Fe-HZSM-5 using ion co-exchange, including alkali metals (Li, Na, K, Cs), alkaline earth metals (Mg, Ca, Ba) and rare-earth metals (La, Ce, Sm), as presented in Figure 2. In comparison with the Fe-HZSM-5 catalyst, promoter doping greatly enhanced NO conversion, and this enhancement is more pronounced in a low temperature range (<400 °C), except for Na, as shown in Figure 2a–c. For alkali metals, K and Cs exhibited a similar enhancement. Ba and Sm were the best for the alkaline earth and rare-earth metals, respectively. By contrast, K, Cs and Ba displayed a much better enhancement at a low temperature (<400 °C). More importantly, the selectivity of by-product NO₂ was significantly decreased due to promoter addition, especially at a low temperature range, as presented in Figure 2d–f. In brief, promoter doping improved the conversion of NO but inhibited the formation of by-product NO₂, resulting in an increase in N₂ selectivity.

Choosing the best promoters (K, Cs, Ba), different doping methods were comparatively investigated, as shown in Figure 3. Taking K doping, for example, K-Fe represents Fe firstly exchanged with HZSM-5, then K. Whereas Fe-K was the opposite exchange order, while Fe/K means Fe and K co-exchanged with HZSM-5. As indicated in Figure 3, metal and promoter exchanging with HZSM-5 one by one is a better method than co-exchange. It can be seen that Fe-K, Cs-Fe and Fe-Ba show a higher NO conversion than the other catalysts.

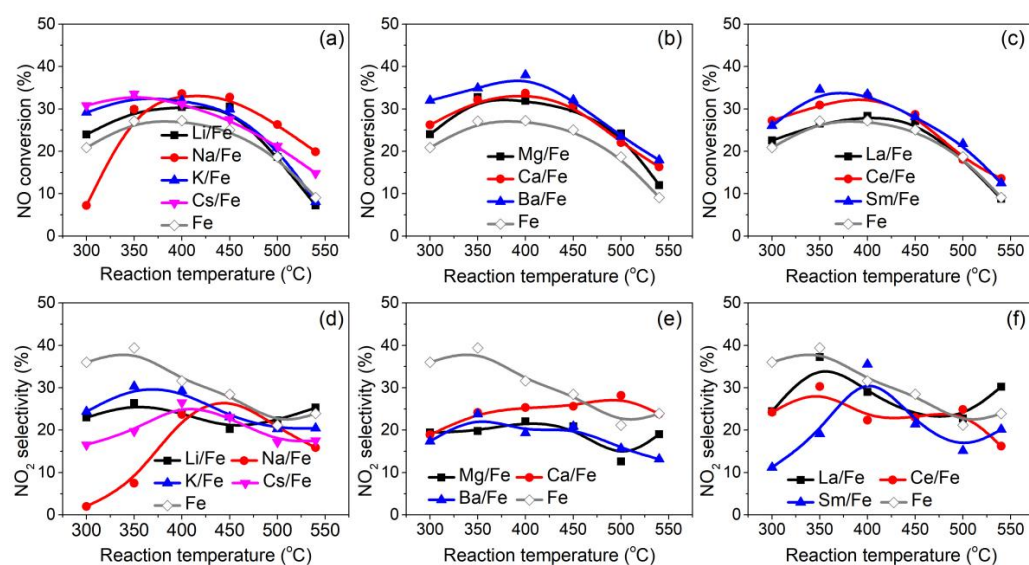


Figure 2. NO conversion and NO₂ selectivity of promoter-doped Fe-HZSM-5: (a,d) alkali metals; (b,e) alkaline earth metals; (c,f) rare-earth metals doping. NO = 1000 ppm, SO₂ = 500 ppm, O₂ = 10 vol.% with N₂ as balance gas, GHSV = 15,000 h⁻¹.

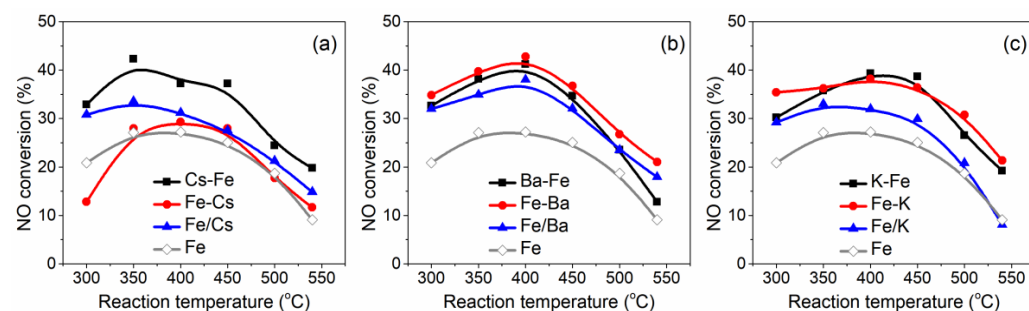


Figure 3. NO conversion of metal-doped Fe-HZSM-5: (a) Cs promoter; (b) Ba promoter; (c) K promoter. NO = 1000 ppm, SO₂ = 500 ppm, O₂ = 10 vol.% with N₂ as balance gas, GHSV = 15,000 h⁻¹.

2.3. SO₂ Resistance of Promoter-Doped Fe-HZSM-5

SO₂ resistance of the catalyst is one of the most important factors for the practical application of DeNO_x for ship exhaust gas. It is generally accepted that SO₂ in exhaust gas can easily poison the catalyst, leading to a quick decrease in the catalytic activity of the catalyst. The Fe-K-HZSM-5, Cs-Fe-HZSM-5 and Fe-Ba-HZSM-5 catalysts all exhibited a high NO conversion, as concluded above. Therefore, the SO₂ resistance of these catalysts was comparatively evaluated with time at 350 °C in the presence of 500 ppm SO₂, as shown in Figure 4. Clearly, the enhancement of the promoter on the activity of Fe-HZSM-5 was confirmed again by the continuous operation. In comparison with Fe-HZSM-5, NO conversion increased from 25% to 45% for Cs-Fe-HZSM-5, increasing by ca. 80%. More importantly, Cs-Fe-HZSM-5 exhibited a better SO₂ resistance, since its NO conversion slightly increased, whereas the NO conversion of Fe-K-HZSM-5 gradually decreased within 10 h of operation. It is worth noting that the catalysts with a high NO conversion correspondingly exhibited a high SO₂ conversion. However, this finding does not apply to the formation of the NO₂ by-product, since Cs-Fe-HZSM-5 displayed a lower selectivity of NO₂ in comparison with Fe-HZSM-5. These phenomena indicate that SO₂ might prefer to deposit on the Cs site, since Cs displays a stronger basicity than Fe, which protects the Fe site from sulfur poisoning to some extent. Therefore, Cs-Fe-HZSM-5 is the best regarding the NO conversion, NO₂ selectivity and SO₂ resistance among the catalysts studied.

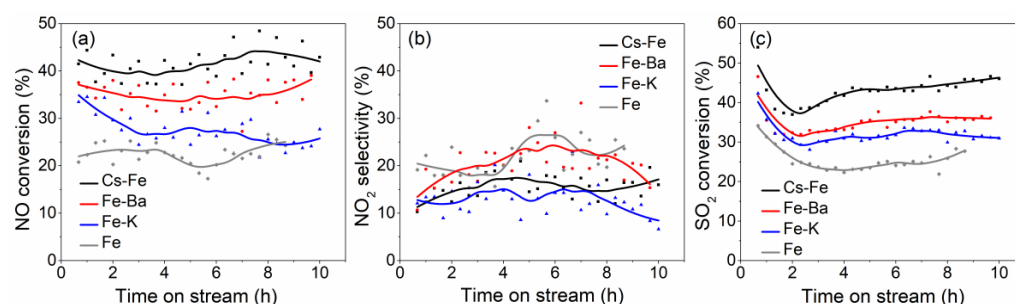


Figure 4. SO₂ resistance of promoter-doped Fe-HZSM-5 at 350 °C: (a) NO conversion; (b) NO₂ selectivity; (c) SO₂ removal. Reaction temperature of 350 °C, NO = 1000 ppm, SO₂ = 500 ppm, O₂ = 10 vol.% with N₂ as balance gas, GHSV = 15,000 h⁻¹.

2.4. Potentials for Improving NO Conversion

Figure 5 showed the potential ways for improving NO conversion. It is worth noting that the Fe/Cs molar ratios and Si/Al molar ratios of HZSM-5 and the exchanged-solution concentration all significantly affect NO conversion. Clearly, NO conversion can be enhanced by increasing the Fe/Cs molar ratio or decreasing the Si/Al molar ratio of HZSM-5 zeolite. Furthermore, increasing the exchanged-solution concentration of Fe nitrate has also been found to be an effective way to improve NO conversion. These findings point out that the number of Fe sites plays an important role in NO conversion, which has been further demonstrated in our recent work, and the related studies will be reported in the near future.

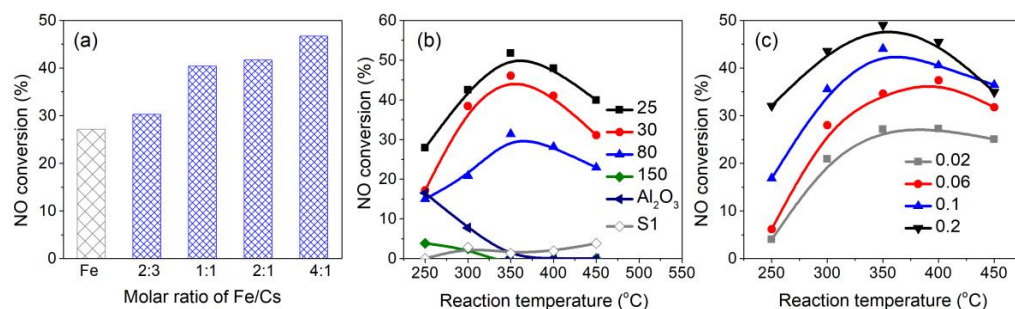


Figure 5. NO conversion of Fe-based HZSM-5 catalyst: (a) Fe/Cs molar ratio; (b) Si/Al molar ratio of HZSM-5; (c) exchange-solution concentration of Fe nitrate. NO = 1000 ppm, SO₂ = 500 ppm, O₂ = 10 vol.% with N₂ as balance gas, GHSV = 15,000 h⁻¹.

3. Discussion

The above-mentioned experimental results show that the Cs-doped Fe-HZSM-5 catalyst exhibited a high NO conversion as well as SO₂ resistance but a low NO₂ selectivity. To understand this phenomenon, a series of characterization techniques including N₂ physisorption, XRD, ICP, XRF, UV-Vis, XPS, NO/SO₂-TPD, H₂-TPR and HAADF-STEM were employed to analyze the physicochemical properties of the Cs-doped Fe-HZSM-5 catalysts.

3.1. Structure-Activity Correlations

Figure 6 and Table 1 present the XRD, UV-Vis, XPS, ICP and XRF results of Cs-Fe-HZSM-5, Fe-Cs-HZSM-5 and Fe/Cs-HZSM-5 catalysts, with Fe-HZSM-5 as a reference. The employed HZSM-5 zeolite has a Si/Al molar ratio of ca. 30, which is determined by XRF in Table 1. XRD patterns reveal that all the metal-exchanged HZSM-5 samples still preserve the typical MFI topology of the HZSM-5 zeolite, because only the diffraction peaks of HZSM-5 have been observed and no additional peaks related to Fe or Cs species appeared, as shown in Figure 6a [25]. However, Fe species existed in HZSM-5, which can be confirmed by ICP in Table 1 and UV-Vis in Figure 6b. Thus, it can be speculated that the Fe species existed in the form of amorphous oxide and were highly dispersed in HZSM-5, so that they

were too small to be detected by XRD. From the UV–Vis results, three $O^{2-} \rightarrow Fe^{3+}$ charge-transfer transitions corresponding to three kinds of Fe oxo species were detected, including isolated Fe^{3+} located at the ion-exchange sites (<300 nm), small oligomeric Fe_xO_y clusters (300–400 nm) and Fe_2O_3 nanoparticles (>400 nm, sub-bands at 470 nm and 560 nm) [26–30]. The Cs-Fe-HZSM-5 sample exhibits the highest amount of isolated Fe^{3+} and oligomeric Fe_xO_y , since the quantity of the Fe species is highly correlated to the absorbance intensity. Generally, binary $Fe^{3+}-O-Fe^{3+}$ (hydroxylated bi-nuclear Fe^{3+} sites) was considered be the major small oligomeric Fe_xO_y species in Fe-exchanged HZSM-5 with a low Fe/Al molar ratio, as shown in Table 1, which is supported by existing reports [27,31].

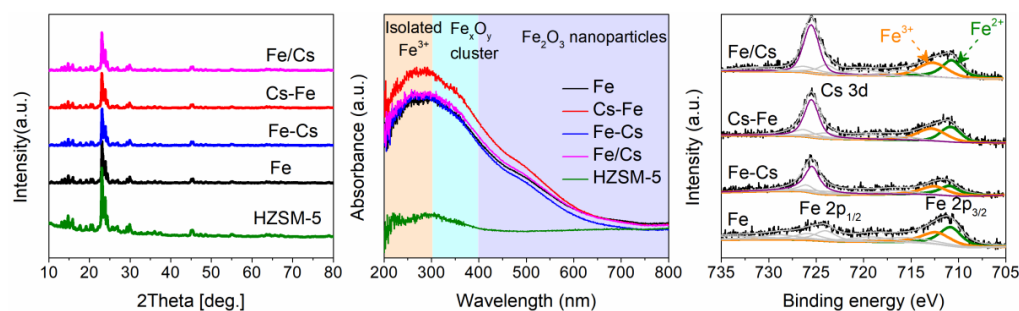


Figure 6. Properties of Fe-HZSM-5, Cs-Fe-HZSM-5, Fe-Cs-HZSM-5 and Fe/Cs-HZSM-5 catalysts analyzed by (a) XRD, (b) UV–Vis and (c) XPS.

Table 1. Composition of Fe-HZSM-5, Cs-Fe-HZSM-5, Fe-Cs-HZSM-5 and Fe/Cs-HZSM-5 catalysts determined by ICP, XRF and XPS.

Samples	ICP			XRF		XPS	
	Fe (wt.%)	Cs (wt.%)	Fe:Cs (mol)	Si:Al (mol)	Fe Atomic (%)	Cs Atomic (%)	Fe ³⁺ Area (%)
Fe	0.590	0	-	28.57	1.23	0	46.59
Cs-Fe	0.610	0.057	25.64	29.58	0.40	0.26	53.77
Fe-Cs	0.367	0.044	20.01	30.04	0.39	0.28	51.80
Fe/Cs	0.373	0.054	16.51	29.98	0.38	0.40	49.56

XPS analysis reveals that the Fe species in Fe-exchanged HZSM-5 existed in both Fe^{3+} and Fe^{2+} , and Cs-doping enhanced the content of the Fe^{3+} species, which is more pronounced in Cs-Fe-HZSM-5, as shown in Figure 6c and Table 1 [32,33]. This can be further confirmed by the H_2 -TPR results in Figure 7a. Two reduction peaks were observed at around 350 °C and 400 °C. The peak at 350 °C was attributed to the reduction of Fe^{3+} in the Fe_2O_3 nanoparticles located in the channels of HZSM-5, whereas the peak at 400 °C was the typical reduction of isolated Fe^{3+} to Fe^{2+} [32,33], which was more evident for Cs-Fe-HZSM-5 in comparison with Fe-HZSM-5. This suggests that Cs doping enhanced the content of the isolated Fe^{3+} species, which is consistent with the UV–Vis results. Figure 7b showed the N_2 adsorption–desorption isotherms for Fe-HZSM-5 with or without Cs modification. Clearly, all the isotherms rose rapidly at $P/P_0 < 0.1$, which is the characteristic of a microporosity material with a type I isotherm. Besides, H4-type hysteresis loops at $0.4 < P/P_0 < 1.0$ were presented for these isotherms, which is indicative of the presence of narrow slit-like pores in these samples [34]. Cs and Fe-exchanged HZSM-5 decreased the narrow slit-like pores of HZSM-5, as shown in Figure 7b, as well as the pore volume, as shown in Figure 7c. Correspondingly, the surface area of HZSM-5 decreased from 362 to 349 m^2/g .

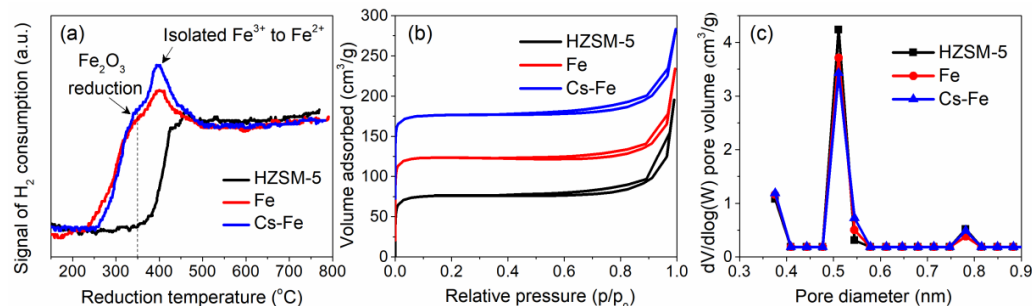
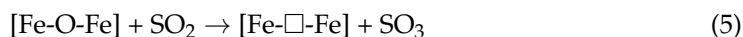
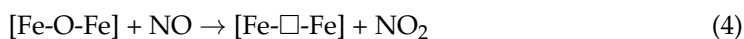
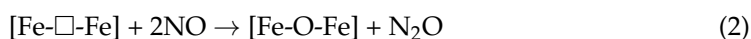


Figure 7. Properties of Cs-Fe-HZSM-5 catalyst analyzed by (a) H₂-TPR, (b) N₂ adsorption/desorption isotherms and (c) pore size distribution. Note: In (b), the offsets of Y axis for HZSM-5, Fe and Cs-Fe were −30, 20 and 70, respectively.

Cs-Fe-HZSM-5 was the best for NO decomposition, though it exhibited the highest amount of isolated Fe³⁺ and Fe³⁺-O-Fe³⁺. These findings indicate that isolated Fe³⁺ species and Fe³⁺-O-Fe³⁺ dimer could be the active sites for NO decomposition through a redox process. The main steps are shown in Equations (1)–(3) (□ representing an oxygen vacancy), which is supported by the reported literature using Cu-exchanged ZSM-5 catalysts [7]. Compared to isolated Fe³⁺, Fe³⁺-O-Fe³⁺ was reported to be more reducible and temperature-dependent, and it was considered to be the main active sites at a high temperature. However, Fe³⁺-O-Fe³⁺ could be dissociated into isolated Fe³⁺ at a temperature as low as 423 K [29]. Therefore, Fe³⁺-O-Fe³⁺ plays an important role in this study regarding the relatively high reaction temperature. In addition, the by-product NO₂ detected in the outlet gas may originate from NO oxidation through Equation (4) [28]. Similarly, Equation (5) could be mainly responsible for the SO₂ conversion, especially at a high temperature.



3.2. Understanding SO₂ Resistance of Promoter-Doped Fe-HZSM-5

As indicated by the continuous operation in Figure 4, significant SO₂ is deposited on the surface of promoter-doped Fe-HZSM-5 catalyst, but it does not decrease the conversion of NO over these catalysts, which is more pronounced for Cs-Fe-HZSM-5 within 10 h. To understand this phenomenon, XPS was employed to analyze the deposited sulfur species, as shown in Figure 8. Clearly, SO₄^{2−} was detected on the catalyst's surface, which can be confirmed by the binding energy of ~170 eV [35–37], indicating that SO₂ was oxidized into SO₄^{2−} during the reaction process. The amount of SO₄^{2−} deposition on the catalyst's surface followed the order of Fe > Cs-Fe > Fe-Ba > Fe-K; meanwhile, the peak of SO₄^{2−} slightly shifted toward a low binding energy in the same order. It is worth noting that Fe and Cs-Fe had a similar amount of SO₄^{2−} deposition, but they exhibited the lowest and the highest NO conversions, respectively, as shown in Figure 4. These experimental results indicate that a part of SO₄^{2−} reacts with the Cs sites in addition to the Fe sites, which protects a portion of the Fe sites from being poisoned by SO₄^{2−}. This can also be supported by the obvious decrease in the Cs signal and Fe signal in Figure 8. Different from the Cs signal, the XPS signals of K and Ba were very weak, but their relative quantities were higher than that of Cs, as determined by the elemental mapping analysis shown in Figure 9. This means that most of the K and Ba existed in the channels of HZSM-5 but not on the surface of catalysts. Therefore, the surface Fe sites deactivated by reacting with SO₄^{2−} and by SO₂/SO₃^{2−} that can be confirmed by a S 2p signal at around 168 eV for the K- and

Ba-doped Fe-HZSM-5 samples [37]. In addition, the Fe species was well-dispersed on Cs-Fe-HZSM-5 in comparison with the samples of the K- and Ba-doped Fe-HZSM-5, as shown in Figure 9. These could be the main reason that the Cs-Fe-HZSM-5 catalyst possessed high NO conversion and SO₂ resistance. Although, if the reaction operates over a much longer period of time, the catalyst would finally be deactivated by the sulfur accumulation.

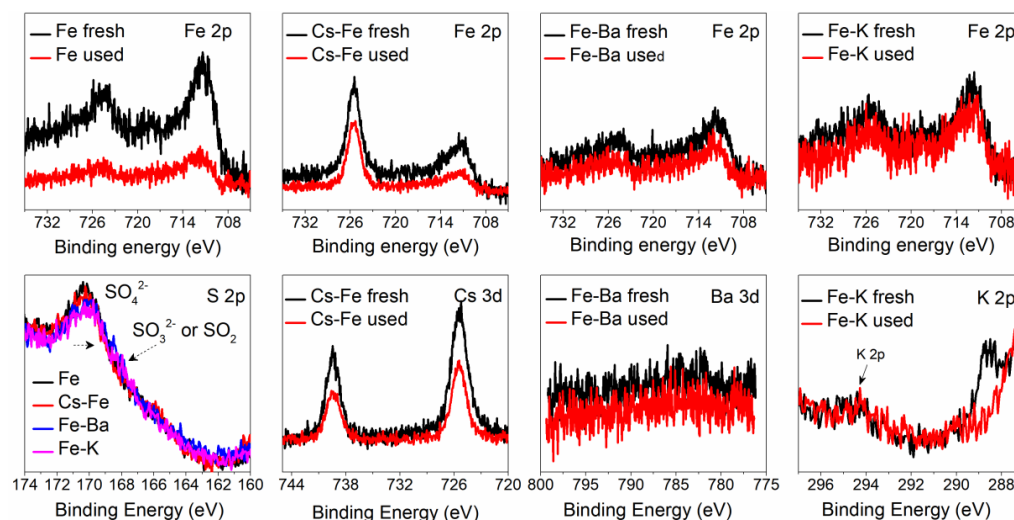


Figure 8. XPS spectra of Cs-, K- and Ba-doped Fe-HZSM-5 catalyst before and after 10 h of continuous reaction.

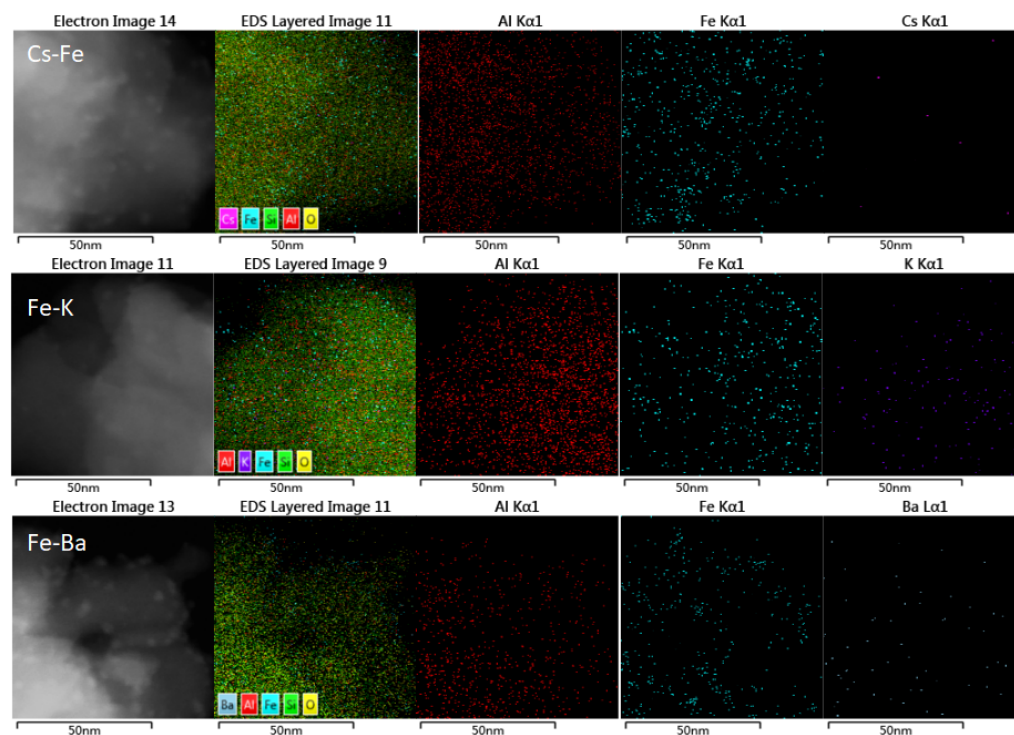


Figure 9. HAADF-STEM images of Cs-, K- and Ba-doped Fe-HZSM-5 with corresponding elemental mapping analysis.

In addition, NO adsorption and NO/SO₂ coadsorption, followed by NO and SO₂ desorption experiments, were performed to further understand the SO₂ resistance of the Cs-Fe-HZSM-5 catalyst, as presented in Figure 10. In the case of only NO adsorption, the Cs modification (Cs-Fe-HZSM-5) obviously enhanced the intensity of the NO adsorption peak at a high temperature (250–400 °C) compared with Fe-HZSM-5. In contrast, in the

case of NO/SO₂ co-adsorption, as shown in Figure 10b, the presence of SO₂ hindered the NO adsorption on both the Fe-HZSM-5 and Cs-Fe-HZSM-5 catalysts at a high temperature (250–400 °C), indicating SO₂ occupied the corresponding Fe sites. This can be further demonstrated by the signal of SO₂ desorption in Figure 10c. Interestingly, compared with the sample of HZSM-5, Fe-HZSM-5 greatly enhanced the adsorption of SO₂, but Cs doping inhibited the SO₂ adsorption, which is supported by the similar SO₂ adsorption amounts of Cs-Fe-HZSM-5 and HZSM-5, as shown in Figure 10c. Therefore, protecting the Fe active site from SO₂ adsorption by Cs doping is one of the reasons for the high NO conversion and SO₂ resistance of the Cs-Fe-HZSM-5 catalyst at 350 °C. Furthermore, the sulfur deposition on the surface of the catalyst mainly existed in the form of metal sulfate for the 10 h operation reaction at 350 °C, because the adsorbed SO₂ species completely desorbed from the catalyst when the temperature was higher than 250 °C, as shown by Figure 10c.

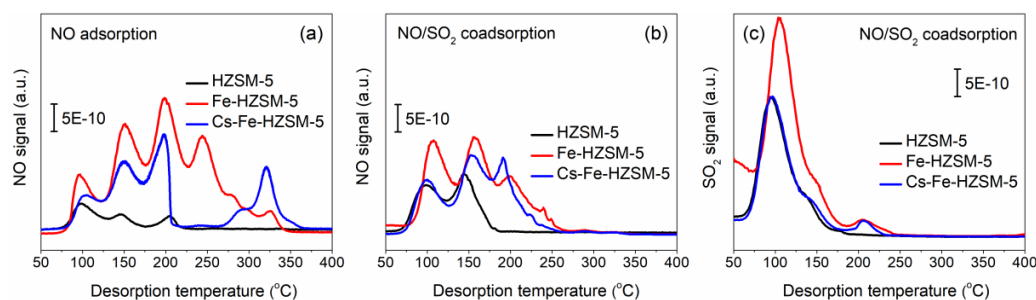


Figure 10. NO and SO₂ TPD profiles of Fe-HZSM-5 and Cs-Fe-HZSM-5: (a) NO desorption profiles after NO adsorption; (b) NO desorption profiles after NO/SO₂ coadsorption; (c) SO₂ desorption profiles after NO/SO₂ coadsorption. 5000 ppm NO with N₂ as balance gas for NO adsorption, 5000 ppm NO, 2500 ppm SO₂ with N₂ as balance gas for NO/SO₂ coadsorption.

4. Materials and Methods

4.1. Materials

4.1.1. Metal-Exchanged Catalyst

The template of the commercial HZSM-5 zeolite with SiO₂/Al₂O₃ = 30 was removed when it was purchased from Nankai University Catalyst Co., Ltd., China. Before use, HZSM-5 was calcined at 400 °C for 2 h to remove the impurities (e.g., adsorbed H₂O). The water absorption of 1 g HZSM-5 was 1.2 mL, which was measured by incipient wetness impregnation. That is, deionized water was added to the 1 g HZSM-5 powder dropwise under stirring, until the 1 g HZSM-5 was completely soaked by water; meanwhile, no extra water was left. In this condition, the amount of the water used was the water absorption of 1 g HZSM-5.

HZSM-5 catalyst was prepared by aqueous-phase ion exchange. Specifically, the precursor metal nitrates (Fe(NO₃)₃·9H₂O, Co(NO₃)₃·6H₂O, Ni(NO₃)₂·6H₂O and Cu(NO₃)₃·3H₂O) were dissolved in deionized water to achieve 0.02 mol/L solution. Then, 6 g HZSM-5 powder was soaked in 14.4 mL metal nitrate solution at 70 °C for 2 h under continuous stirring (2.4 mL/g HZSM-5). Next, the resulting mixture was filtered and washed with deionized water until pH of the filtrate was around 7, and the process was repeated twice. Subsequently, the paste was dried at 120 °C for 5 h before being calcined in air at 540 °C for 4 h. The resulting sample was pressed and sieved into 20–40 mesh for activity test.

4.1.2. Promoter-Doped Fe-HZSM-5 Catalyst

The M-Fe-HZSM-5 catalyst was prepared in two steps. The first step was to obtain Fe-HZSM-5 using the above-described procedures (4.1.1). The second step was as follows. The resulting Fe-HZSM-5 sample was dispersed in 14.4 ml 0.01 mol/L metal nitrate solution to obtain 1:2 molar ratio of M to Fe, and the suspension was stirred at 70 °C for 2 h, followed by filtering and washing with deionized water. Finally, the paste was dried at 120 °C for 5 h, before being calcined in air at 540 °C for 4 h. The Fe-M-HZSM-5 catalyst was prepared using a similar process as M-Fe-HZSM-5. Differently, the promoter M firstly exchanged

with HZSM-5 to obtain M-HZSM-5. After that, the Fe exchanged with M-HZSM-5. The M/Fe-HZSM-5 catalyst means that promoter M and Fe co-exchanged with HZSM-5. The preparation process was similar to that described in 4.1.1, but the difference is that the precursors of promoter and iron nitrate were dissolved in deionized water together.

4.2. Catalyst Characterization

N₂-physisorption was performed on a BET apparatus (Micromeritics Tristar II2020, Atlanta, GE, USA) to measure the physical properties of catalyst materials, such as internal and external specific surface area, pore size distribution and pore volume. The specific surface area was calculated by Brunauer–Emmett–Teller (BET) formula. A 0.15–0.2 g sample was firstly treated in vacuum at room temperature for 30 min and then heated to 350 °C for 5 h to remove the impurities. Finally, nitrogen adsorption and desorption were carried out under the temperature of liquid nitrogen, and the physical adsorption curve of the catalyst was obtained. X-ray diffraction (XRD) was recorded on a Rigaku D-Max 2400 (25 mA, 40 kV), with Cu-K_α ray from 5–80° and a scanning speed of 10°/min. X-ray photoelectron spectroscopy (XPS) was achieved on an ESCALAB XI+ (UK) using the Al K_α ray source (150 W), with 500 μm plate size, 50 eV energy of passage and 0.05 eV of energy step. X-ray fluorescence spectroscopy (XRF) data were recorded on a S8 TICER X (BRUKER AXS, DE) to analyze the composition of the catalysts. H₂ temperature programmed reduction (H₂-TPR) test was conducted on a Quantachrome Chem BET 3000 system to analyze the redox properties of the catalysts. A 0.15 g sample was firstly pretreated at 550 °C for 1 h in N₂ atmosphere to remove impurities such as H₂O and CO₂ adsorbed on the surface of the catalysts. After cooling to 50 °C, the temperature was raised from 50 °C to 800 °C at a rate of 10 °C/min in 10 vol.%H₂/Ar atmosphere, and the signal of H₂ consumption was collected. Diffuse reflectance UV–Vis spectroscopy (DR UV–Vis) was achieved on an Agilent UV-550 photometer. NO-TPD and NO/SO₂-TPD data were recorded using an on-line mass spectrometry (Decra gas analysis mass spectrometer, Hiden Company, Warrington, UK) connected with the reactor for the catalyst test. A 1 g catalyst was firstly pretreated in an argon flow (50 mL/min) at 540 °C for two hours. Then, the sample was cooled to 50 °C, and 5000 ppm NO with N₂ as balance gas (or a mixture of 5000 ppm NO and 2500 ppm SO₂ with N₂ as balance gas) was adsorbed with a flow rate of 100 mL/min at 50 °C for 30 min. After that, the adsorbed sample was degassed at 50 °C in Ar atmosphere with a flow rate of 100 mL/min for 0.5 h. Finally, the sample was heated from 50 °C to 750 °C at a rate of 10 °C/min, during which the desorbed NO and SO₂ were recorded by MS with a SEM detector.

4.3. Activity and Sulfur Resistance of Catalysts

The NO decomposition performance of the prepared catalysts was carried out in a continuous-flow fixed-bed quartz reactor under the simulated ship exhaust of 1000 ppm NO, 500 ppm SO₂ and 10 vol.% O₂ with N₂ as a balance gas, as shown in Figure 11. The simulated gas mixture was fed to 2 g catalyst with 20–40 mesh at a total flow rate of 60 L/h, and the corresponding gas space velocity was 15,000 h⁻¹. Specifically, before the test, the catalyst was in situ heated to 300 °C, and then the activity data were collected from 300 °C to 550 °C at an interval of 50 °C. The sulfur resistance was tested in a similar way, but the difference is that the reaction temperature was maintained at 350 °C and the activity data were collected at an interval of 0.5 h. The inlet and outlet gas composition were monitored using a Madur IR Photon II analyzer (Austria, madur Photon Infrared gas analyser). It is worth noting that a small amount of NO₂ was detected to be around 70–80 ppm in the above simulated feed gas. In addition, no N₂O was produced, and NO₂ was the only by-product observed in this study. Thus, the indicators of catalyst evaluation mainly include NO conversion, SO₂ removal and the selectivity of N₂, which were calculated according to the following equations.

$$\text{NO conversion (\%)} = \frac{[\text{NO}]_{\text{in}} - [\text{NO}]_{\text{out}}}{[\text{NO}]_{\text{in}}} \times 100\% \quad (6)$$

$$\text{SO}_2 \text{ conversion (\%)} = \frac{[\text{SO}_2]_{\text{in}} - [\text{SO}_2]_{\text{out}}}{[\text{SO}_2]_{\text{in}}} \times 100\% \quad (7)$$

$$\text{NO}_2 \text{ selectivity (\%)} = \frac{[\text{NO}_2]_{\text{out}} - [\text{NO}_2]_{\text{in}}}{[\text{NO}]_{\text{in}} - [\text{NO}]_{\text{out}}} \times 100\% \quad (8)$$

$$\text{N}_2 \text{ selectivity (\%)} = 100\% - \text{NO}_2 \text{ selectivity (\%)} \quad (9)$$

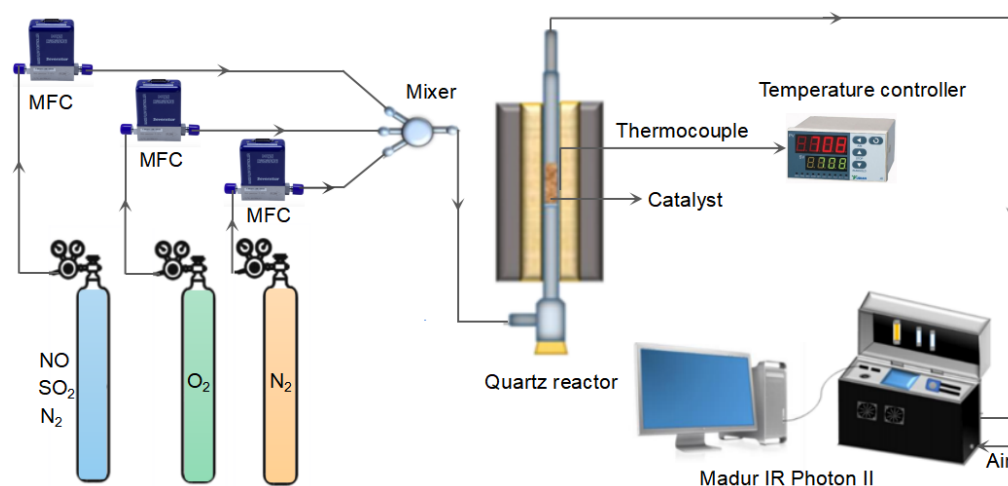


Figure 11. Schematic of the experimental setup for NO decomposition catalytic test.

5. Conclusions

A series of metal-exchanged HZSM-5 catalysts were prepared and evaluated for the NO decomposition that occurred in simulated ship exhaust gas with 1000 ppm NO, 500 ppm SO₂ and 10 vol.% O₂ with N₂ as the balance gas. Fe was found to be the most active metal. Cs, Ba and K were found to be better promoters at improving the low-temperature activity of Fe-HZSM-5, among Li, Na, K, Cs, Mg, Ca, Ba, La, Ce and Sm. In addition, the NO conversion was greatly facilitated by increasing the exchange-solution concentration and Fe/Cs molar ratio as well as by lowering the Si/Al molar ratio. The Cs-Fe-HZSM-5 catalysts show a high NO conversion and SO₂ conversion but a low selectivity of the NO₂ by-product within 10 h of continuous operation. This indicates that the Cs-Fe-HZSM-5 catalyst has a relatively high SO₂ resistance. The catalyst characterization results (N₂ physisorption, XRD, ICP, XRF, UV-Vis, XPS, NO/SO₂-TPD, H₂-TPR and HAADF-STEM) show that SO₄²⁻ was the major species deposited on the catalyst's surface. Cs doping not only inhibited the SO₂ adsorption on Fe-HZSM-5 but also enhanced the Fe dispersion and increased the isolated Fe and Fe-O-Fe species. These could be the primary reasons for the high NO conversion and SO₂ resistance as well as the low NO₂ selectivity observed over Cs-Fe-HZSM-5 for NO decomposition.

Author Contributions: Conceptualization, F.W. and L.W.; methodology, F.W., P.L. and J.G.; software, K.X. and Y.Z. (Yanrui Zhang); validation, K.X., Y.Z. (Yanrui Zhang) and L.W.; formal analysis, Y.Y.; investigation, F.W. and P.L.; resources, Y.Z. (Yimin Zhu) and L.W.; data curation, F.W.; writing—original draft preparation, F.W.; writing—review and editing, Y.Y. and L.W.; visualization, J.G. and L.W.; supervision, Y.Z. (Yimin Zhu) and L.W.; project administration, L.W.; funding acquisition, L.W. All authors have read and agreed to the published version of the manuscript.

Funding: This research was funded by the LiaoNing Revitalization Talents Program (No. XLYC1907008), the Fundamental Research Funds for the Central Universities (No. 3132021165) and the key Science and Technology Project List of Ministry of Transport of the People's Republic of China (No. 2020-MS4-108).

Data Availability Statement: The data are available from corresponding authors based on reasonable requirement.

Conflicts of Interest: The authors declare no conflict of interest.

References

1. Zhao, J.; Wei, Q.; Wang, S.; Ren, X. Progress of ship exhaust gas control technology. *Sci. Total Environ.* **2021**, *799*, 149437. [[CrossRef](#)] [[PubMed](#)]
2. Wan, Z.; Zhu, M.; Chen, S.; Sperling, D. Pollution: Three steps to a green shipping industry. *Nature* **2016**, *530*, 275–277. [[CrossRef](#)]
3. Jimenez, V.J.; Kim, H.; Munim, Z.H. A review of ship energy efficiency research and directions towards emission reduction in the maritime industry. *J. Clean. Prod.* **2022**, *366*, 132888. [[CrossRef](#)]
4. IMO. *Annex VI of MARPOL 73/78: Regulations for the Prevention of Air Pollution from Ships and NOx Technical Code*; Marine Environment Protection Committee: London, UK, 1997.
5. Fritz, A.; Pitchon, V. The current state of research on automotive lean NOx catalysis. *Appl. Catal. B Environ.* **1997**, *13*, 1–25. [[CrossRef](#)]
6. Glick, H.S.; Klein, J.J.; Squire, W. Single-Pulse Shock Tube Studies of the Kinetics of the Reaction $N_2 + O_2 \rightleftharpoons 2NO$ between 2000–3000° K. *J. Chem. Phys.* **1957**, *27*, 850–857. [[CrossRef](#)]
7. Zhang, Y.; Cao, G.; Yang, X. Advances in De-NOx Methods and Catalysts for Direct Catalytic Decomposition of NO: A Review. *Energy Fuels* **2021**, *35*, 6443–6464. [[CrossRef](#)]
8. Xie, P.; Ji, W.; Li, Y. NO direct decomposition: Progress, challenges and opportunities. *Catal. Sci. Technol.* **2021**, *11*, 374–391. [[CrossRef](#)]
9. Shen, Q.; Dong, S.; Li, S.; Yang, G.; Pan, X. A Review on the Catalytic Decomposition of NO by Perovskite-Type Oxides. *Catalysts* **2021**, *11*, 622. [[CrossRef](#)]
10. Zhang, R.; Liu, N. Selective Transformation of Various Nitrogen-Containing Exhaust Gases toward N_2 over Zeolite Catalysts. *Chem. Rev.* **2016**, *116*, 3658–3721. [[CrossRef](#)]
11. Iwamoto, M.; Furukawa, H.; Mine, Y.; Uemura, F. Copper (II) Ion-exchanged ZSM-5 Zeolites as Highly Active Catalysts for Direct and Continuous Decomposition of Nitrogen Monoxide. *J. Chem. Soc. Chem. Commun.* **1986**, *16*, 1272–1273. [[CrossRef](#)]
12. Iwamoto, M.; Furukawa, H. Removal of Nitrogen Monoxide through a Novel Catalytic Process. 1. Decomposition on Excessively Copper Ion Exchanged ZSM-5 Zeolites. *J. Phys. Chem.* **1991**, *95*, 3727–3730. [[CrossRef](#)]
13. Zhang, K.; Yu, F.; Zhu, M. Enhanced Low Temperature NO Reduction Performance via MnOx-Fe₂O₃/Vermiculite Monolithic Honeycomb Catalysts. *Catalysts* **2018**, *8*, 100. [[CrossRef](#)]
14. Zhu, N.; Shan, W.; Lian, Z.; Zhang, Y. A superior Fe-V-Ti catalyst with high activity and SO₂ resistance for the selective catalytic reduction of NOx with NH₃. *J. Hazard. Mater.* **2020**, *382*, 120970. [[CrossRef](#)]
15. Yu, Y.; Tan, W.; An, D.; Wang, X. Insight into the SO₂ resistance mechanism on γ -Fe₂O₃ catalyst in NH₃-SCR reaction: A collaborated experimental and DFT study. *Appl. Catal. B Environ.* **2021**, *281*, 119544. [[CrossRef](#)]
16. Kang, T.H.; Youn, S.; Kim, D.H. Improved catalytic performance and resistance to SO₂ over V₂O₅-WO₃/TiO₂ catalyst physically mixed with Fe₂O₃ for low-temperature NH₃-SCR. *Catal. Today* **2021**, *376*, 95–103. [[CrossRef](#)]
17. Yao, G.; Wei, Y.; Gui, K.; Ling, X. Catalytic performance and reaction mechanisms of NO removal with NH₃ at low and medium temperatures on Mn-W-Sb modified siderite catalysts. *J. Environ. Sci.* **2022**, *115*, 126–139. [[CrossRef](#)]
18. Guo, K.; Fan, G.; Gu, D.; Yu, S. Pore Size Expansion Accelerates Ammonium Bisulfate Decomposition for Improved Sulfur Resistance in Low-Temperature NH₃-SCR. *ACS Appl. Mater. Interfaces* **2019**, *11*, 4900–4907. [[CrossRef](#)]
19. Wu, G.; Liu, S.; Chen, Z.; Yu, Q. Promotion effect of alkaline leaching on the catalytic performance over Cu/Fe-SSZ-13 catalyst for selective catalytic reduction of NOx with NH₃. *J. Taiwan Inst. Chem. E* **2022**, *134*, 104355. [[CrossRef](#)]
20. Liu, Z.; Su, H.; Chen, B. Activity enhancement of WO₃ modified Fe₂O₃ catalyst for the selective catalytic reduction of NO by NH₃. *Chem. Eng. J.* **2016**, *299*, 255–262. [[CrossRef](#)]
21. Kawakami, K.; Ogura, M. Theoretical investigation of novel two-step decomposition of nitric oxide over Fe(II) ion-exchanged zeolites using DFT calculations. *Catal. Today* **2015**, *242*, 343–350. [[CrossRef](#)]
22. Ohnishi, T.; Kawakami, K. Direct decomposition of NO on metal-loaded zeolites with coexistence of oxygen and water vapor under unsteady-state conditions by NO concentration and microwave rapid heating. *Catal. Today* **2017**, *281*, 566–574. [[CrossRef](#)]
23. Shi, S.; Li, M.; Ge, C. Insights into adsorption performances and direct decomposition mechanisms of NO on [FeO]¹⁺-ZSM-5: A density functional theory study. *Appl. Surf. Sci.* **2020**, *508*, 145212. [[CrossRef](#)]
24. Wang, H.; Li, X. Preparation and evaluation of iron nanoparticles embedded CNTs grown on ZSM-5 as catalysts for NO decomposition. *Chem. Eng. J.* **2020**, *392*, 123798. [[CrossRef](#)]
25. Fan, L.; Song, L. Direct conversion of CH₄ to oxy-organics by N₂O using freeze-drying FeZSM-5. *Chem. Eng. J.* **2019**, *369*, 522–528. [[CrossRef](#)]
26. Liu, Q.; Bian, C.; Jin, Y. Influence of calcination temperature on the evolution of Fe species over Fe-SSZ-13 catalyst for the NH₃-SCR of NO. *Catal. Today* **2022**, *388–389*, 158–167. [[CrossRef](#)]
27. Grünert, W.; Ganesh, P.K. Active Sites of the Selective Catalytic Reduction of NO by NH₃ over Fe-ZSM-5: Combining Reaction Kinetics with Postcatalytic Mössbauer Spectroscopy at Cryogenic Temperatures. *ACS Catal.* **2020**, *10*, 3119–3130. [[CrossRef](#)]

28. Gao, F.; Zheng, Y. Iron Loading Effects in Fe/SSZ-13 NH₃-SCR Catalysts: Nature of the Fe Ions and Structure–Function Relationships. *ACS Catal.* **2016**, *6*, 2939–2954. [[CrossRef](#)]
29. Kim, J.; Jentys, A.; Maier, S.M. Characterization of Fe-Exchanged BEA Zeolite Under NH₃ Selective Catalytic Reduction Conditions. *J. Phys. Chem. C* **2013**, *117*, 986–993. [[CrossRef](#)]
30. Li, S.; Wang, Y.; Wu, T. First-Principles Analysis of Site- and Condition-Dependent Fe Speciation in SSZ-13 and Implications for Catalyst Optimization. *ACS Catal.* **2018**, *8*, 10119–10130. [[CrossRef](#)]
31. Iwasaki, M.; Shinjoh, H. NO evolution reaction with NO₂ adsorption over Fe/ZSM-5: In situ FT-IR observation and relationships with Fe sites. *J. Catal.* **2010**, *273*, 29–38. [[CrossRef](#)]
32. You, Y.; Chen, S.; Li, J. Low-temperature selective catalytic reduction of N₂O by CO over Fe-ZSM-5 catalysts in the presence of O₂. *J. Hazard. Mater.* **2020**, *383*, 121117. [[CrossRef](#)] [[PubMed](#)]
33. Zeng, J.; Chen, S.; Fan, Z. Simultaneous Selective Catalytic Reduction of NO and N₂O by NH₃ over Fe-Zeolite Catalysts. *Ind. Eng. Chem. Res.* **2020**, *59*, 19500–19509. [[CrossRef](#)]
34. Sing, K.S.W.; Everett, D.H.; Haul, R.A.W.; Moscou, L.; Pierotti, R.A.; Rouquerol, J.; Siemieniowska, T. Reporting physisorption data for gas/solid systems with special reference to the determination of surface area and porosity. *Pure Appl. Chem.* **1985**, *57*, 603–619. [[CrossRef](#)]
35. Chi, N. FeS redox power motor for PDS continuous generation of active radicals on efficient degradation and removal of diclofenac: Role of ultrasonic. *Chemosphere* **2022**, *300*, 134574. [[CrossRef](#)]
36. Wu, Y.; Xing, D.; Zhang, L. Application of a novel heterogeneous sulfite activation with copper(i) sulfide (Cu₂S) for efficient iohexol abatement. *RSC Adv.* **2022**, *12*, 8009–8018. [[CrossRef](#)]
37. Yong, X.; Chen, H. Insight into SO₂ poisoning and regeneration of one-pot synthesized Cu-SSZ-13 catalyst for selective reduction of NO by NH₃. *Chin. J. Chem. Eng.* **2022**, *46*, 184–193. [[CrossRef](#)]